Stoichiometry dependence of hardness, elastic properties, and oxidation resistance in TiN/SiN$_x$ nanocomposites deposited by a hybrid process

F.-J. Haug, P. Schwaller, J. Wloka,[a] and J. Patscheider[b]
Swiss Federal Laboratories for Material Testing and Research (EMPA), Überlandstrasse 129, CH 8600 Dübendorf, Switzerland

A. Karimi
Swiss Federal Institute of Technology (EPFL), Faculty of Basic Science, CH-1015 Lausanne, Switzerland

M. Tobler
IonBond AG Olten, Industriestrasse 211, CH-4600 Olten, Switzerland

(Received 9 January 2004; accepted 26 April 2004; published 9 July 2004)

TiN/SiN$_x$ nanocomposite layers with Si contents between 0 and 25 at. % were deposited by a reactive arc-magnetron sputtering hybrid process. The stoichiometry of the SiN$_x$ phase was found to be related to the silicon sputter target state, i.e., elemental or nitrided. TiN/SiN$_x$ layers with a Si:N ratio close to 0.75 (silicon nitride) show a hardness maximum at overall Si contents between 5 and 7 at. %. The hardness maximum is absent for nitrogen deficient stoichiometries of SiN$_x$. The oxidation resistance of the composite layers is three to five times better than that of pure TiN. In contrast to the effect of the stoichiometry on hardness, the oxidation resistance depends on the overall silicon content only, regardless of stoichiometry. © *2004 American Vacuum Society.*
[DOI: 10.1116/1.1763907]

I. INTRODUCTION

Nanocomposite materials like TiN/SiN$_x$ show properties which are a direct consequence of their nanostructure. Owing to the limited miscibility of TiN and SiN$_x$,[1] the microstructure of the TiN/SiN$_x$ compound is characterized by nanocrystalline TiN grains with sizes between 5 and 20 nm which are embedded in a matrix of amorphous SiN$_x$.[2,3] Such nanocomposite materials show increased hardness compared to the constituent compounds because for small grain size the deformation mechanism is governed by grain boundary sliding rather than dislocation movement.[2] Hardness values approaching that of diamond have been reported for the TiN/SiN$_x$ system.[4] The addition of SiN$_x$ also results in an improved oxidation resistance compared to pure TiN.[5,6] Both effects make these materials interesting for advanced protective coatings because hardness and oxidation resistance are equally important for wear resistance and result in a prolonged lifetime of coated tools.

Composite layers of TiN/SiN$_x$ have been grown by various methods like plasma assisted chemical vapor deposition (PACVD)[2,7] and reactive magnetron sputtering.[3,5] For industrial applications, however, the deposition by cathodic arc evaporation has several advantages; it is a robust process, it yields high growth rates, and its high degree of ionization allows one to control the energy of impinging ions by the application of a bias voltage. Unfortunately, silicon cannot be evaporated by arc processes due to its brittleness and low electric conductivity. Sputter processes are more suitable for the deposition of silicon. Recently, arc deposition of titanium and sputtering of silicon have been successfully combined in hybrid processes for the deposition of TiN/SiN$_x$[8–10] and (Ti,Al)N/SiN$_x$.[11,12]

An often experienced difficulty in reactive sputtering of insulating materials is the formation of compounds on the surface of the sputter target. The phenomenon is usually referred to as target poisoning and lowers the deposition rates for two reasons: (i) compounds usually have higher binding energies and thus lower sputtering yields per impinging ion; and (ii) compounds have higher secondary electron yields which consume much of the energy for electron emission instead of the preferred sputtering of material.[13] Also, target poisoning is not desirable because of unstable operation and arcing.

In this investigation we studied the influence of the target state on the stoichiometry of TiN/SiN$_x$ composite coatings grown by an arc-magnetron hybrid process and how the stoichiometry of the SiN$_x$ phase influences the properties of the composite material.

II. EXPERIMENT

TiN/SiN$_x$ layers were deposited in a cylindrical vacuum chamber which is pumped by a turbomolecular pump (300 l/s). The base pressure of the system is in the low 10^{-4} Pa region. Silicon is sputtered in dc mode from an unbalanced magnetron (UBM) sputtering source. The target size is 88×304 mm^2, for better conductivity it consists of boron-doped polycrystalline Silicon bonded to the cooling plate of the magnetron. Titanium is eroded from a cylindrical arc source with a diameter of 64 mm mounted at an angle of 90° with respect to the silicon target. In all experiments described here the arc current was kept constant at 50 A for the duration of the deposition.

[a]Present address: Department of Materials Science, KLO, University of Erlangen, D-91058 Erlangen, Germany.
[b]Author to whom correspondence should be addressed; electronic mail: joerg.patscheider@empa.ch

The sputter gas supply is controlled by mass flow controllers. The inlet for nitrogen is mounted close to the arc target, argon is supplied through a distributing ring around the silicon sputter target in order to control the nitrogen poisoning of the target. A similar geometry for separate supplies of nitrogen and argon has previously been reported.[14] During the growth the pressure was typically between 0.45 and 0.65 Pa. Target poisoning was identified by a drop in target voltage at constant output power.

The layers were grown onto Si(100) substrates mounted on a substrate holder with planetary rotation. When the silicon target was operated in the nitrided mode, the erosion rate dropped significantly. In these cases the sample rotation was not used. Instead, a stationary substrate position close to the silicon target at maintained total deposition rate was chosen. The deposition time was 1 h for all samples presented in this investigation, the layer thickness varies within 1.5 and 2.0 μm.

Before each deposition the temperature in the reactor was raised to 200 °C by radiation heaters. During the growth of the layer it increased to about 300 °C by additional heating of the plasma process. The substrates were electrically biased with −500 V during the first 2 min for the deposition of a Ti sticking layer in pure argon atmosphere. Then, nitrogen was added and the bias was changed to the desired value for the layer deposition, either −100 or −200 V.

The compositions of the layers and the chemical states of the constituent elements were measured with x-ray photoelectron spectroscopy (XPS) using a Shirley background subtraction. The crystallographic orientation of the layers was investigated with x-ray diffraction (XRD) in θ–2θ configuration. The full width at half maximum (FWHM) of the (200) reflex was used for the determination of the crystallite size according to the Scherrer formula. Wherever possible the second-order reflex was used to separate the effects of grain size and stress on the broadening by an analysis according to Williamson and Hall.[15,16] Hardness and Young's modulus of the layers were measured by nanoindentation with a Berkovich indenter and evaluated according to the procedure of Oliver and Pharr. Care was taken to restrict the evaluation to indentation depths less than 10% of the layer thickness in order to avoid influences of the substrate. The presence of droplets due to the arc process results in some scattering of the hardness and elastic data. The presented values are the averages of 15 to 20 indentation measurements, the shown error bars represent the corresponding standard deviations. The oxidation resistance of the TiN/SiN_x layers was investigated by measuring the thickness of the oxide layer after annealing at temperatures between 700 and 800 °C. This temperature range represents a compromise between low oxidation rates of TiN/SiN_x below 600 °C and too fast oxidation rates for Si-free TiN. The thickness of the oxide cap was measured either by XPS sputter profiling in case of thin layers or by grinding of a spherical calotte for thicker layers. Oxide layers between 400 and 700 nm were measured with both methods; the thickness values of these films were used to calibrate the sputter profiles.

TABLE I. Deposition parameters of the two sample sets.

	$[Si_3N_4]/[Si]$ (from XPS)	Substrate position	Total flux of N_2 [sccm][a]
Set 1	<0.5, "elemental"	Planetary rotation	<20
Set 2	0.6–0.8, "nitrided"	Stationary in front of Si target	20–24

[a]8–10 sccm N_2 are consumed by the Ti arc source (see the text).

III. RESULTS AND DISCUSSION

Two sets of TiN/SiN_x samples with different stoichiometries of the SiN_x phase were produced for the investigation of hardness and elastic properties. Depending on the nitrogen/argon mixture, silicon was sputtered from either an elemental or a nitrided target surface. In the following these two conditions will be referred to as "set 1" (elemental target) and "set 2" (nitrided target), the deposition conditions of the two sets are summarized in Table I. Owing to its higher reactivity, the titanium arc target was in nitrided state under both conditions except for extremely nitrogen-depleted cases which are not considered here.

Figure 1 shows the current–voltage characteristics of the Si magnetron target alone, i.e., without the operation of the arc source. With increasing nitrogen partial pressure the slopes of the characteristics become steeper, a given target voltage results in increasingly higher discharge currents due to the enhanced excitation of secondary electrons from the nitrided surface. The close relationship between target voltage and poisoning state of the target surface is well documented and has also been successfully employed for the control of reactive sputter processes.[13,17]

Owing to the high pumping speed, the hysteresis effects observed in Fig. 1 are rather weak. Regions of negative differential resistance as, for example, reported for the reactive deposition of aluminum nitride[18] or silicon oxide,[19] were not

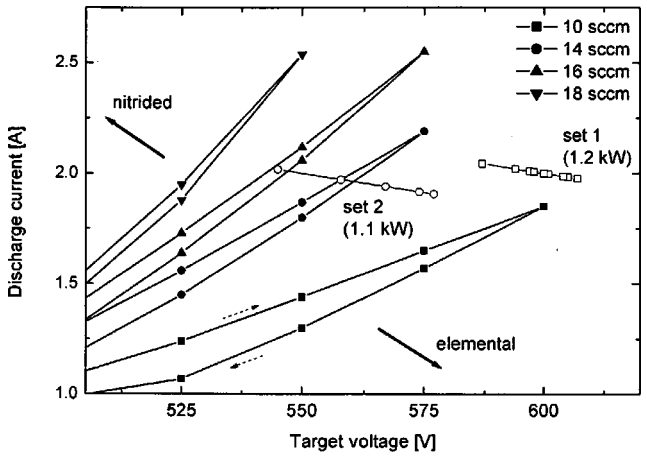

FIG. 1. Hysteresis curves of the silicon target at different fluxes of nitrogen. The total pressure was kept between 0.61 and 0.66 Pa. Increasing and decreasing target voltages result in the upper and lower branches, respectively (dashed arrows). The discharge parameters for typical samples of set 1 and set 2 are included. The Si content of samples of the shown processes is approximately the same at 8 at. %.

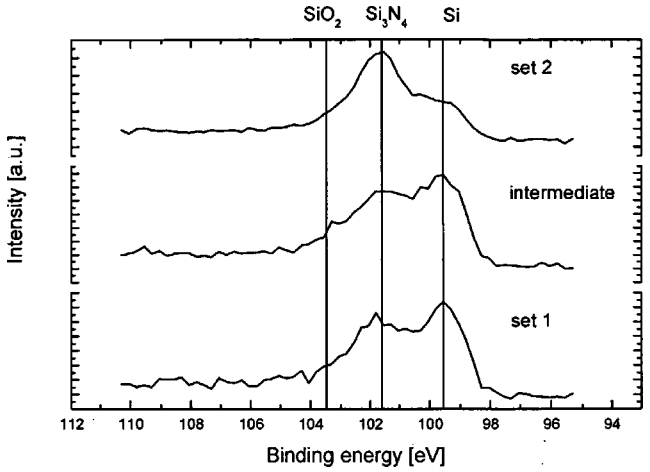

FIG. 2. XPS spectra of the Si $2p$ binding energy for typical samples of set 1 (bottom), set 2 (top), and intermediate conditions (middle). The spectra are dominated by contributions of elemental Si at 99.6 eV, silicon nitride and 101.7 eV, and a shoulder due to silicon oxide at 103.5 eV.

observed. Thus, in the absence of unstable switching between elemental and poisoned state of operation the target voltage turned out to be a useful gauge for assessing the nitridation state of the target.

A. Stoichiometry of the SiN_x matrix

Figure 1 includes discharge parameters of the Si target which were recorded during typical depositions. The variations in voltage and current reflect systematic changes in the process characteristics like the warming up of targets, temporary instabilities due to retriggering of the arc, etc. Figure 1 illustrates that for set 1 the discharge parameter correspond to a target state with little nitridation. In contrast, for set 2 lower target voltages and higher discharge currents indicate discharge conditions of a nitrided target. The Si $2p$ photoelectron spectra of three illustrative samples are shown in Fig. 2. The spectra are dominated by two main contributions at 99.6 and 101.7 eV, and a small contribution at 103.5 eV. These binding energies are identified with elemental Si, silicon nitride, and silicon oxide, respectively. The presence of elemental silicon is surprising since the formation of titanium silicide would seem more likely and has been reported in case of TiN/SiN_x nanocomposites grown by plasma CVD.[20] However, the corresponding shift of the Si $2p$ peak in the range from 0.4 to 0.6 eV with respect to elemental Si at 99.6 eV[21,22] is not observed in Fig. 2.

We conclude that the chemical state of the silicon present in the TiN/SiN_x composites reflects the state of the silicon target; samples of set 1 are sputtered from a predominantly elemental target surface and contain silicon predominantly in elemental form. Similarly, samples of set 2 contain predominantly silicon nitride because they are sputtered from the nitrided target. Thus, a correlation between the target state (i.e., elemental or nitrided) and the ratio of elemental silicon to silicon nitride in the composite layer is observed despite the fact that the discharge characteristics of the sputtering target may be quite different when the Si target is operated with and without arc source. Conversely, if a certain composition is desired, it is necessary to meet the required target conditions by adjusting the nitrogen flux. The actual value of the nitrogen flux is only of secondary importance. For example, in the hybrid process a typical arc current of 50 A results in a nitrogen consumption corresponding to nitrogen fluxes between 8 and 10 sccm. Accordingly, the total nitrogen flux during the hybrid process had to be increased to 18 or 20 sccm.

Also, when there are phases of unstable arc operation like the warming up phase at the beginning of each deposition or during times of retriggering, there are noticeable changes in the nitrogen partial pressure. Such changes are observed to immediately alter the current–voltage characteristic of the silicon target. Due to the constant power control mode during the deposition, the readings of discharge current I_D and target voltage V_T are then located on branches of hyperbolas ($I_D \times V_T = P = \text{const}$) as displayed in Fig. 1 for P equal to 1.1 and 1.2 kW.

Figures 1 and 2 illustrate that the formation and the stoichiometry of SiN_x in the composite layer critically depend on the state of the silicon target. It appears that the nitridation of silicon is only achieved via the formation of silicon nitride on the surface of the sputter target and subsequent sputtering of the compound.

A second potential reaction path for the formation of SiN_x would be sputtering of elemental silicon and reaction with nitrogen on the sample surface. The acceleration of positive ions in the field of the biased sample should be sufficient to result in impact dissociation and the production of reactive atomic nitrogen.[23] However, a variation of the sample bias voltage between -25 and -250 V at constant silicon sputtering conditions did not show any significant influence on the stoichiometry of SiN_x. Higher bias voltages are not practical for arc-magnetron hybrid processes because resputtering of silicon by accelerated titanium ions has been reported to lower the silicon content in the layers.[9,10]

Finally, the possibility of reactions in the plasma should be considered. The target–substrate distance in the configuration with planetary rotation varies between 5 and 25 cm. The mean free path for elastic collisions between argon and nitrogen is estimated to be about 2 cm. Ionization or dissociation of N_2 by collisions or electron impact requires threshold energies of at least 9.7 eV, the dissociation energy of nitrogen. This value is above the mean electron energies which are around 5 eV or less.[24] Also, cross sections of ionizing and dissociative collisions are about one order of magnitude lower than those of elastic collisions.[23] Thus, dissociation of nitrogen in regions other than the cathode sheath of the silicon target or the vicinity of the arc source and substrate seem unlikely for this chamber geometry and the chosen pressure.

B. Structural characterization of the TiN/SiN_x layers

The structural properties of the TiN/SiN_x layers were investigated by x-ray diffration in θ–2θ mode. Figure 3 shows that layers of pure TiN and TiN/SiN_x composites with low Si

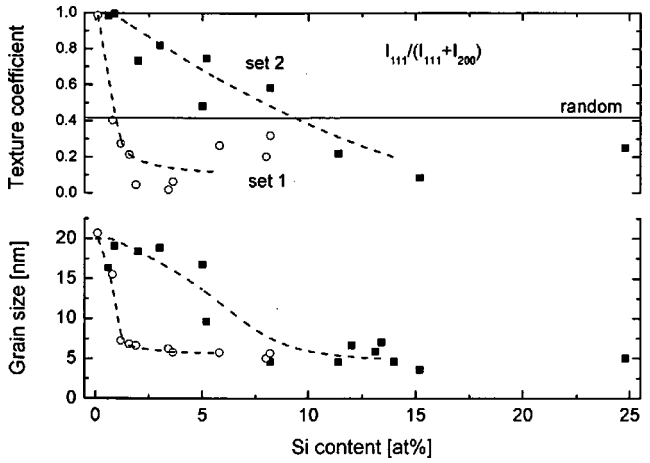

FIG. 3. Dependence of texture (top) and grain size (bottom) of the TiN crystallites in the SiN_x matrix. Open symbols denote layers where silicon has been sputtered from the elemental target (set 1), closed symbols correspond to layers of set 2 where silicon is predominantly in the nitride binding.

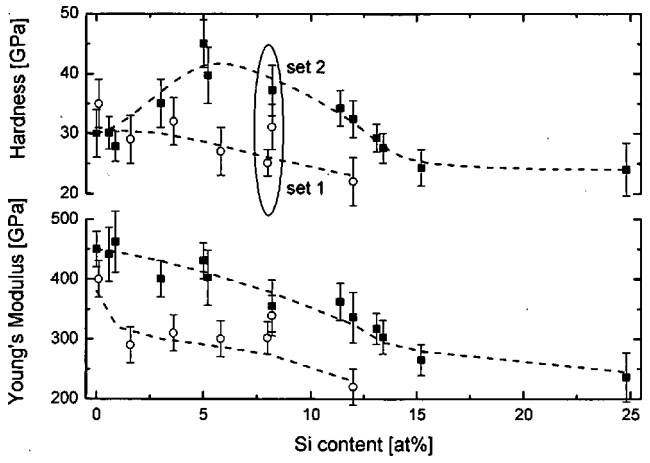

FIG. 4. Hardness (top) and Young's modulus (bottom) of TiN/SiN_x composite layers in dependence of the Si content. Open symbols denote values measured on set 1, closed symbols represent samples of set 2. The highlighted hardness values at 8 at. % correspond to the three samples shown in Fig. 2.

contents are predominantly textured in the (111) direction. For higher Si contents the texture changes to (200). It appears that for the sputtering from the nitrided target (set 2) the transition between the two preferred textures takes place at higher Si contents but the data scatter considerably. Changes of the texture from (111) to (200) with increasing Si content have been reported for TiN/SiN_x layers deposited by arc-magnetron hybrid processes[9,14] and were also observed for other deposition processes like PACVD[7] and UBM sputtering.[25]

The average size of the TiN crystallites in TiN/SiN_x layers has been determined from the (200) reflection which is present in all diffractograms. Figure 3 shows the dependence of the grain size as obtained by application of the Scherrer formula to the FWHM data, assuming a structure factor K equal to 1. The grain size is reduced from about 20 nm in layers of pure TiN to values between 5 and 10 nm for higher silicon contents. Again, the transition between the two regions is shifted toward higher silicon contents when silicon is sputtered from the nitrided target (set 2). Compared to the results evaluated according to the Scherrer formula, the results of the Williamson–Hall analysis yield grain sizes that are about twice as large. The remaining part of the reflex broadening is attributed to tensile stress perpendicular to the substrate as determined by XRD. This is in fact a result of compressive stress parallel to the substrate surface. Using the values of Young's modulus from the indentation measurements, an average stress on the order of 2 GPa is estimated. Due to substrate effects the values of the Young's modulus are often underestimated, thus, the stress in the investigated layers could be higher, even up to reported values between 3 and 5 GPa.[9,26]

C. Mechanical properties of the TiN/SiN_x layers

Hardness and Young's modulus of the two sample sets are presented in Fig. 4. For Si contents below 1 at. % hardness and Young's modulus scatter from 30 to 35 GPa and from 400 to 450 GPa, respectively. The reported hardness values of TiN layers grown by arc PVD[9] and other methods[2,5] are in the range from 25 to 27 GPa. Values for the Young's modulus vary between 350 GPa[2] and 480 GPa.[5]

With increasing Si content in the layer the hardness of the samples of set 1 (elemental silicon target) decreases. For the Young's modulus a very similar decrease is observed. For the samples of set 2 (nitrided silicon target) the behavior is quite different. For Si contents between 5 and 7 at. % there is a hardness maximum around 40 GPa. Toward higher Si contents the hardness decreases and approaches the value of Si_3N_4 at 23 GPa. The behavior is indicative of hardening due to the formation of a nanocrystalline/amorphous composite material which is distinguished by three regions: (i) for low contents of the amorphous phase (SiN_x) the hardness is similar to the bulk value of the first phase (TiN) because deformations proceed via dislocation movement in large grains, similar to bulk material. (ii) For a content of the second phase where all grains are fully percolated, dislocation movement within the TiN grains is precluded, deformations are only possible by grain boundary sliding with a corresponding increase of hardness. (iii) For higher contents of the amorphous phase the hardness is governed by the deformation mechanism of the amorphous phase alone.[26]

The Young's modulus of set 2 decreases monotonically from 450 to 280 GPa for a Si content of 25 at. %. The absence of an increase at the position of the hardness maximum clearly rules out stress hardening, rather it supports the finding of a hardening mechanism due to nanostructure effects, i.e., small grain size in combination with full percolation of the grains in an amorphous matrix. This important finding is corroborated by the x-ray diffraction analysis of Sec. III B where stresses in the order of 2 GPa were found which are independent of the Si content.[27]

The three samples which are highlighted in Fig. 4 underline that next to grain size and percolation the correct sto-

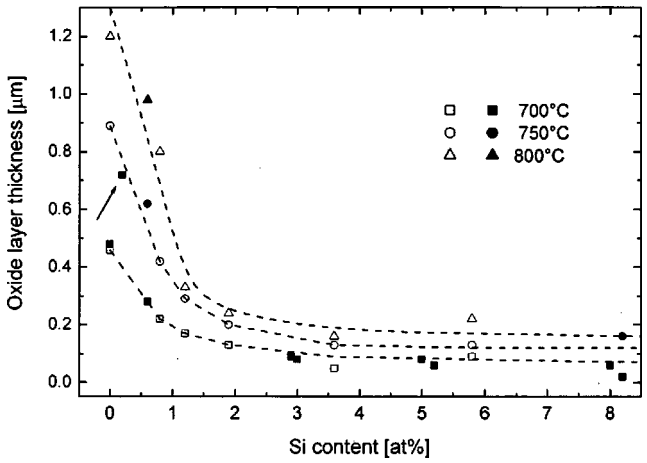

FIG. 5. Thickness of the TiO_2 layer on top of the TiN/SiN_x composite layer after annealing for 10 min in air. The oxidation resistance is improved by a factor of 3–5 for Si contents exceeding 2 at. %. Closed symbols correspond to measurements of set 1, open symbols denote results from set 2. Except for one incidence (arrow) the stoichiometry does not show any influence on oxidation resistance.

ichiometry of the SiN_x phase emerges as the third prerequisite for improved hardness in TiN/SiN_x. Figures 2 and 3 show that within measurement accuracy these samples have the same grain sizes and Si contents but the contribution of Si_3N_4 to the Si signal is most pronounced in the sample belonging to set 2 (nitrided target), which is also the sample with the highest hardness. The hardness increase is attributed to a better cross linking and therefore stronger bonding in the silicon-nitrogen network. If silicon is not sufficiently nitrided the hardness increase is absent and the hardness of the composite material exhibits the behavior that is expected for a mixture of TiN with a material softer than Si_3N_4, e.g., titanium silicide (8.5 GPa[28,29]) or silicon (between 10 and 13 GPa[30]).

D. Oxidation resistance

The oxidation resistance of TiN/SiN_x layers was studied in the temperature range from 700 to 800 °C. Samples with silicon contents ranging from 0 to 8 at. % were annealed at three different temperatures in air. An annealing time of 10 min was chosen for two reasons: (a) for low Si contents too long annealing times would result in a complete conversion of TiN into TiO_2; and (b) too low annealing times result in poor accuracy, particularly on the thin oxide layers on samples with high Si content. Figure 5 shows the thickness of TiO_2 layer on top of the layers. The oxidation resistance is improved by a factor of 3–5 for all Si contents exceeding 2 at. %. The two sample sets show identical TiO_2 overlayer thickness, there is no observable influence of the SiN_x stoichiometry on the oxidation resistance.

Detailed oxidation experiments on UBM sputtered TiN/SiN_x composite layers showed that the oxidation involves two different mechanisms.[5] It is shown that up to 850 °C the oxidation in layers with a silicon content of 14 at. % is limited by diffusion of oxygen through the protecting Si_3N_4 layer, the oxidation proceeds with an apparent activation energy of 43 kJ/mol. At higher temperatures a second oxidation mechanism is reported where titanium is thought to diffuse to the interface and subsequently form TiO_2.[5] This mechanism shows higher activation energies between 200 and 300 kJ/mol, depending on the microstructure of the layer. This second mechanism is reported to be operative in the whole investigated temperature range for a layer with a lower silicon content of 5 at. % and also for pure TiN.[5]

The oxidation experiments shown in Fig. 5 were performed for silicon contents lower than 8 at. % and only at three different temperatures. As far as the determination is meaningful from the available data, the activation energies vary between 150 and 280 kJ/mol suggesting an oxidation mechanism which is governed by the diffusion of titanium to the interface rather than the diffusion of oxygen into the layer. This conclusion is corroborated by the finding that the oxidation process is independent of the SiN_x stoichiometry in the layer.

IV. CONCLUSIONS

We have prepared TiN/SiN_x nanocomposite layers with a hybrid process that combines arc evaporation and magnetron sputtering. By choosing appropriate nitridation conditions of the silicon sputter target it is possible to control the stoichiometry of the silicon nitride phase in the layer. Hardness measurements showed that a hardness increase typical for nanocomposites is only found in case of a sufficiently nitrided SiN_x phase. For poor nitridation the hardness increase is absent. Compared to pure TiN the oxidation resistance of the composite material is improved by a factor of 3–5 for silicon contents exceeding 2 at. %. In contrast to the hardness, the oxidation resistance depends only on the absolute Si content and not its nitridation state. The oxidation behavior can be explained within existing oxidation models.

ACKNOWLEDGMENT

Support from the Swiss Commission for Technology and Innovation (CTI) within the TOP NANO 21 program under Contract No. 5304.1 is gratefully acknowledged.

[1]P. Rogl and J. Schuster, *Phase Diagrams of Ternary Boron Nitride and Silicon Nitride Systems* (ASM International, Materials Park, OH, 1992).
[2]S. Vepřek *et al.*, Surf. Coat. Technol. **86/87**, 394 (1996).
[3]F. Vaz *et al.*, Surf. Coat. Technol. **133/134**, 307 (2000).
[4]S. Vepřek, J. Vac. Sci. Technol. A **17**, 2401 (1999).
[5]M. Diserens, J. Patscheider, and F. Lévy, Surf. Coat. Technol. **120/121**, 158 (1999).
[6]R. Cremer and D. Neuschütz, Surf. Coat. Technol. **146/147**, 229 (2001).
[7]B. H. Park, Y.-I. Kim, and K. H. Kim, Thin Solid Films **348**, 210 (1999).
[8]S. H. Kim, J. K. Kim, and K. H. Kim, Thin Solid Films **420/421**, 360 (2002).
[9]P. J. Martin and A. Bendavid, Surf. Coat. Technol. **163/164**, 245 (2003).
[10]S. R. Choi, I.-W. Park, S. H. Kim, and K. H. Kim, Thin Solid Films **447/448**, 371 (2004).
[11]I.-W. Park, S. R. Choi, M.-H. Lee, and K. H. Kim, J. Vac. Sci. Technol. A **21**, 895 (2003).
[12]P. Holubar, M. Jilek, and M. Sima, Surf. Coat. Technol. **133/134**, 145 (2000).
[13]I. Safi, Surf. Coat. Technol. **127**, 203 (2000).

[14]K. H. Kim, S. R. Choi, and S.-Y. Yoon, Surf. Coat. Technol. **161**, 243 (2002).
[15]W. H. Hall, Proc. Phys. Soc., London, Sect. A **62**, 741 (1949).
[16]G. K. Williamson and W. H. Hall, Acta Metall. **1**, 22 (1953).
[17]J. Chapin and C. R. Condon, U.S. Patent No. 4,166,748, 1979.
[18]J. Affnito and R. R. Parsons, J. Vac. Sci. Technol. A **2**, 1275 (1984).
[19]K. Steenbeck, E. Steinbeiß, and K. D. Ufert, Thin Solid Films **92**, 371 (1982).
[20]S. Veprˇek *et al.*, Surf. Coat. Technol. **133/134**, 152 (2000).
[21]S. M. Lee *et al.*, Nucl. Instrum. Methods Phys. Res. B **157**, 220 (1999).
[22]S. A. Chambers *et al.*, Phys. Rev. B **35**, 634 (1987).
[23]K. S. Fancey, Vacuum **46**, 695 (1995).
[24]C. H. Shon *et al.*, IEEE Trans. Plasma Sci. **26**, 1635 (1998).
[25]M. Diserens, J. Patscheider, and F. Lèvy, Surf. Coat. Technol. **108/109**, 241 (1998).
[26]W.-J. Chou, G.-P. Yu, and J.-H. Huang, Surf. Coat. Technol. **149**, 7 (2002).
[27]J. Patscheider, T. Zehnder, and M. Diserens, Surf. Coat. Technol. **146/147**, 201 (2001).
[28]R. Radhakrishnan, C. H. Henager, Jr., J. L. Brimhall, and S. B. Bhaduri, Scr. Mater. **34**, 1809 (1996).
[29]I. J. Shon, H. C. Kim, D. H. Rho, and Z. A. Munir, Mater. Sci. Eng., A **269**, 129 (1999).
[30]B. Bhushan and X. Li, J. Mater. Res. **12**, 54 (1997).